

Free Vibration Analysis of Rotating Functionally-Graded Cantilever Beams

M. N. V. Ramesh

Department of Mechanical Engineering, Nalla Malla Reddy Engineering College, Hyderabad-500088, India

N. Mohan Rao

Department of Mechanical Engineering, JNTUK College of Engineering Vizianagaram, Vizianagaram-535003, India

(Received 23 May 2012; accepted 20 August 2013)

The increasing needs of the industry involved in development of components for aerospace and power sector demand the engineering community to develop new concepts and strategies to improve the functional requirements of structures and to enhance the strength of materials. This is particularly essential in the cases of rotating beams that are subjected to severe vibration under large pressure loadings, high rotating accelerations, centrifugal forces, geometric stiffening, etc. A theoretical investigation of the free vibration characteristics of rotating cantilever beams, made of a functionally-graded material (FGM) consisting of metal and alumina, is presented in this study. It was assumed that the material properties of the FGM beam were symmetric, but varied continuously in the thickness direction from the core at the mid section to the outer surfaces, according to a power-law relation. Equations of motion were derived from a modelling method, which employed the hybrid deformation variable. The natural frequencies were determined using the Rayleigh-Ritz method. The effect of parameters such as the power law index, the hub radius, and the rotational speed on the natural frequencies of functionally-graded rotating cantilever beams were examined through numerical studies and then compared with the numerical results reported in earlier works.

NOMENCLATURE

\vec{a}^P	Acceleration vector of the generic point P	U	Strain energy of the functionally-graded beam
A	Cross-sectional area of the beam	\vec{v}^O	Velocity of point O
b	Width of the beam	\vec{v}^P	Velocity vector of the generic point P
$E_{(z)}$	Young's modulus	x	Spatial variable
h	Total thickness of the beam	γ	Ratio of the angular speed of the beam to the reference angular speed
$\hat{i}, \hat{j}, \hat{k}$	Orthogonal unit vectors fixed to the rigid hub	δ	Hub radius ratio
J_{11}^E	Axial rigidity of the beam	Θ	Constant column matrix characterizing the deflection shape for synchronous motion
J_{11}^P	Mass density per unit length	μ_1, μ_2, μ_3	Number of assumed modes corresponding to $q_{1i}, q_{2i},$ and q_{3i}
$J_{22,yy}^E, J_{22,zz}^E$	Flexural rigidities of the functionally-graded beam	τ	Dimensionless time
L	Length of the beam	$\phi_{1j}, \phi_{2j}, \phi_{3j}$	Modal functions for s, v and w
n	Power law index	$\vec{\omega}^A$	Angular velocity of the frame A
\vec{P}	Vector from point O to P_0	Ω	Angular speed of the rigid hub
$P_{(z)}$	Effective material property	$(')$	Partial derivative of the symbol with respect to the integral domain variable
$P_{(m)}$	Metallic material property	$('')$	Second derivative of the symbol with respect to the integral domain variable
$P_{(c)}$	Ceramic material property		
q_{1i}, q_{2i}, q_{3i}	Generalized co-ordinates		
r	Radius of the rigid frame		
$\rho_{(z)}$	Mass density per unit volume		
s	Arc length stretch of the neutral axis		
T	Reference period		
u, v, w	Cartesian variables in the directions of $\hat{i}, \hat{j},$ and, \hat{k}		

1. INTRODUCTION

Functionally-graded materials are special composites whose properties change spatially in one or more directions. Functionally-graded structures are being widely applied in extremely high temperature environments like those occurring

around space vehicles, aircrafts, nuclear power plants, automobiles, combustion chambers, turbine blades, etc. As these structures are often subjected to vibration with large pressure loadings, temperature gradients, and thermo-elastically-induced loading, understanding of their dynamic behaviour is important. FGM have been presented as an alternative to laminated composite materials that exhibit a mismatch in properties at the material's interface. The discontinuity in these materials leads to large stress concentrations or intensity factors, attenuation of stress waves, and potentially the commencement and propagation of cracks. This problem was reduced in the FGM because of the gradual change in mechanical properties as a function of position through the composite laminate.

Several studies have been conducted to analyse static and dynamic behaviour of the functionally-graded beams, plates, and shells over the past two decades. In 1994, Naguleswaran considered the doubly-symmetric Euler-Bernoulli uniform beam to describe the lateral vibrations of the beam. Different combinations of the boundary conditions were considered for estimating the first three dimensionless natural frequencies.¹ Sankar, in 2001, presented an elasticity solution based on the Euler-Bernoulli beam theory for a functionally-graded beam subjected to sinusoidal transverse loads, by assuming that property of the beam varied exponentially through the thickness.² In 2009, Sina et al. carried out a free vibration analysis of functionally-graded beams using a new beam theory that differed from the traditional first order shear deformation theory. In this work, Hamilton's principle was used to derive the equations of motion. Different boundary conditions were considered and comparisons were made considering the different beam theories.³ Yang and Chen, in 2008, investigated free vibration and elastic buckling of functionally-graded beams with the material properties varying along the thickness. This was done according to the exponential distributions with open edge cracks through consideration of the Bernoulli-Euler theory and the theoretical spring model.⁴ Ying et al., in 2008, presented the exact two-dimensional elasticity solutions for the bending and free vibration of functionally-graded beams on a Winkler-Pasternak foundation. Infinite trigonometric series were considered to expand the solutions of stresses and displacements.⁵ In 2008 Li suggested a new unified approach for analysing the static and dynamic behaviours of functionally-graded beams, including rotary inertia and shear deformation.⁶

In the same year, Yang et al. investigated the free and forced vibrations of slender FGM beams with open edge cracks under the combined action of an axial compression and a concentrated transverse moving load with different end supports.⁷ Li and Shi, in 2009, employed the extension of the state-space-based differential quadrature method (SSDQM), to study the free vibration of a functionally-graded piezoelectric material (FGPM), multi-layered beam under different boundary conditions. The influence of material parameters on the natural frequency of the FGPM beam was also discussed.⁸ Kadoli et al., in 2008, implemented a displacement field based on the higher order shear deformation theory, to study the static behaviour of

functionally-graded metal-ceramic beams under ambient temperature.⁹

Aydogdu and Taskin, in 2007, investigated the free vibration of a simply-supported functionally-graded beam using classical beam theory, parabolic shear deformation beam theory, and exponential shear deformation beam theory. The governing equations of the beam were derived using the Hamilton principle and the Navier type solution method.¹⁰ In 2006, Kocatürk and Şimşek analysed the lateral vibrations of a beam subjected to eccentric compressive force and harmonically-varying transverse concentrated moving force, using Bernoulli-Euler beam theory. The results of the numerical simulations were presented in various combinations for the value of the eccentricity, the eccentric compressive force, the excitation frequency, and the constant velocity of the transverse moving harmonic force.¹¹ Şimşek and Kocatürk, in 2009, also investigated free and forced vibration of a functionally-graded, simply-supported beam subjected to a concentrated moving harmonic load.

The space-dependent functions were chosen as polynomial functions. The system of equations was derived using Lagrange's equations, under the assumptions of the Euler-Bernoulli beam theory. The material properties of the beam were assumed to vary continuously in the thickness direction, according to an exponential law and a power law. The effects of the distribution of materials with differing properties, the velocity of the moving harmonic load, and the excitation frequency on the dynamic responses of the beam are discussed in this paper.¹² A theoretical model for the free vibration analysis of layered, functionally-graded beams was presented by Kapuria et al., in 2008, and has been validated experimentally.¹³ Jaworski and Dowell, also in 2008, conducted a theoretical and experimental investigation on the flexural-free vibration of a cantilevered beam with multiple cross-section steps; these results were then compared.¹⁴ Kang and Li, in 2009, investigated the mechanical behaviours of a non-linear, functionally-graded, material cantilever beam subjected to an end force, by using large and small deformation theories. The effects of varying the Young's modulus and the non-linearity parameter on the large and small deflections were presented.¹⁵

In the 2008, Benatta et al. presented high-order, flexural theories for short, functionally-graded, symmetric beams under three-point bending. The governing equations were obtained using the principle of virtual work (PVW).¹⁶ In 2009, Şimşek carried out a static analysis of a functionally-graded (FG), simply-supported beam, subjected to a uniformly distributed load using the Ritz method. The analysis was carried out considering the Timoshenko and the higher order shear deformation beam theories. Trigonometric functions were taken as trial functions to describe the transverse, the axial deflections, and the rotation of the cross-section.¹⁷ In 2010, Şimşek also investigated vibration of a functionally-graded (FG), simply-supported beam due to a moving mass, using the Euler-Bernoulli, the Timoshenko, and the third order shear deformation beam theories. In this study, the effects of shear de-

formation, material distribution, velocity of the moving mass, inertia, Coriolis, the centripetal effects of the moving mass on the dynamic displacements, and the stresses of the beam are discussed using Lagrange's equations to derive the system of equations of motion.¹⁸

Ozdemir Ozgumus and Kaya, in 2010, presented a flap-wise bending vibration analysis of a rotating, tapered, Timoshenko beam where the Differential Transform Method (DTM) was used as the tool to obtain the solution.¹⁹ Chih-Ling Huang, in 2009, proposed a method based on the power series solution to estimate the flap-wise vibrations of the rotating Euler beam with constant angular speed.²⁰ Huang et al., in 2010, investigated the natural frequencies of a rotating beam for the flap-wise bending vibration and coupled lag-wise bending and axial vibration. The power series solution was proposed for a very slender rotating beam at high angular velocity to estimate the natural frequency.²¹ Yoo and Shin, in 1998, presented the equations of motion for a rotating cantilever beam based on a new dynamic modelling method. The derived linear equations were used for vibration analysis.²² In 1995, Yoo et al. presented a modelling method for beams undergoing large overall motions and small deformations. In the equations of motion, a quadratic form of the strain energy expressed with the hybrid set of deformation variables in the equations of motion, to obtain the generalized active forces and Cartesian variables, was used to carry out the generalized inertia forces.²³

Park et al., in 2010, employed the constrained multi-body technique to derive equations of motion for a wind-turbine (rotating) blade and numerical problems were solved to verify the accuracy of the proposed method.²⁴ Alshorbagy et al., in 2011, evaluated the dynamic characteristics of a stationary functionally-graded beam considering the material gradation in the axial and transverse directions through the power law-based thickness. The system of equations of motion were derived using the principle of virtual work for the Euler-Bernoulli beam model.²⁵ Fazelzadeh et al., in 2007, and Fazelzadeh and Hosseini, in 2007, investigated a thin-walled beam made of functionally-graded material (FGM). They focused mainly on the aerothermoelastic effects related to graded properties.^{26,27} Piovan and Sampaio, in 2009, developed a rotating, nonlinear model that accounted for the arbitrary axial deformations in a FGM rotating beam; the model was also employed to analyse the isotropic and composite materials.²⁸

To those authors' knowledge, an analysis of the natural frequencies for a functionally-graded rotating beam, considering the rotating accelerations, the centrifugal force, the hub radius, and the material morphology, has scarcely been reported. In this paper, the dynamic modelling method—which is proposed for a homogeneous, rotating cantilever and uses the hybrid deformation variables—is extended to estimate the natural frequencies of a functionally-graded, rotating cantilever beam.²² The governing equations of motion derived for both stretching and bending configurations were observed to be coupled through gyroscopic coupling terms. The present work investigates the effect of power law index, angular speed, and hub

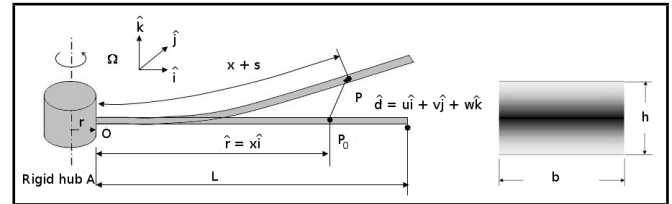


Figure 1: Configuration of the functionally-graded rotating beam.

radius on the natural frequencies of a functionally-graded rotating beam for the bending configuration. This was done by neglecting the coupling effects in the chord-wise and flap-wise modes through numerical studies, and a comparison was made with the numerical results reported in the literature.

2. FUNCTIONALLY-GRADED BEAM

Consider a functionally-graded beam with length L , width b , total thickness h , and composed of a metallic core and ceramic surfaces, as shown in Fig. (1). The graded material properties vary symmetrically along the thickness direction from the core towards the surface, according to a power law:

$$P_{(z)} = P_{(m)} + (P_{(c)} - P_{(m)}) \left| \frac{2 \times z}{h} \right|^2; \quad (1)$$

where $P_{(z)}$ represents an effective material property (i.e., density, $\rho_{(z)}$ or Young's modulus, $E_{(z)}$), and $P_{(m)}$, and $P_{(c)}$ are metallic and ceramic properties, respectively.

The volume fraction exponent, or power law index, n , is a variable whose value is greater than or equal to zero; the variation in beam properties depends on its magnitude. The beam was constructed with the functionally-graded material, which is ceramically rich at the top and bottom surfaces (at $z = \frac{h}{2}$ and $-\frac{h}{2}$) with a protective metallic core (at $z = 0$).

2.1. Equations of Motion

For the problem considered in this study, the equations of motion were obtained under assumptions; namely, that the material properties varied only along the thickness direction according to a power law, and that the neutral and centroidal axes in the cross-section beam coincided. Therefore, the effects due to eccentricity and torsion were not considered. Shear and rotary inertia effects of the beam were also not addressed. No external force acts upon the FG beam, and the beam was attached to a rigid hub that rotated with constant angular speed.

Figure (1) shows the deformation of the neutral axis of a beam fixed to a rigid hub rotating about the axis \hat{k} . The rotation of the beam was characterized by means of a prescribed rotation $\Omega(t)$ around the \hat{k} -axis. The position of a generic point on the neutral axis of the FG beam located at P_0 (before deformation) changed to P (after deformation) and its elastic deformation was denoted as \hat{d} with three components in three-dimensional space. Conventionally, the differential equations of motion were derived by approximating the three Cartesian variables u , v , and w . In the present work, a hybrid set of

Cartesian variables (v and w) and the non-Cartesian variable (s) were approximated by spatial functions. Corresponding coordinates were employed to derive the equations of motion.

2.1.1. Approximation of deformable variables

By employing the Rayleigh-Ritz method, the deformation variables were approximated as follows:

$$s(x, t) = \sum_{j=1}^{\mu_1} \phi_{1j}(x)q_{1j}(t); \quad (2)$$

$$v(x, t) = \sum_{j=1}^{\mu_2} \phi_{2j}(x)q_{2j}(t); \quad (3)$$

and

$$w(x, t) = \sum_{j=1}^{\mu_3} \phi_{3j}(x)q_{3j}(t). \quad (4)$$

In the above equations, ϕ_{1j} , ϕ_{2j} , and ϕ_{3j} were the assumed modal functions for s , v , and w , respectively. Any compact set of functions that satisfy the essential boundary conditions of the cantilever beam can be used as the test functions. The q_{ij} s were the generalized coordinates and μ_1 , μ_2 , and μ_3 were the number of assumed modes used for s , v , and w , respectively. The total number of modes, μ , was equal to the sum of individual modes; i.e., $\mu = \mu_1 + \mu_2 + \mu_3$. The geometric relation between the arc length stretch s and the Cartesian variables u , v , and w were given as Eqs. (5) to (7)²³

$$x + s = \int_0^x \left[\left(1 + \frac{\partial u}{\partial \sigma}\right)^2 + \left(\frac{\partial v}{\partial \sigma}\right)^2 + \left(\frac{\partial w}{\partial \sigma}\right)^2 \right]^{\frac{1}{2}} d\sigma; \quad (5)$$

Based on the assumptions described in section 2.1., the equations of motion were obtained from the following equation:

$$\int_0^L J_{11}^{\rho} \left(\frac{\partial \vec{v}^p}{\partial \dot{q}_i} \right) \vec{a}^p dx + \frac{\partial U}{\partial q_i} = 0; \quad (8)$$

where

$$J_{11}^{\rho} = \int_A \rho_{(z)} dA; \quad (9)$$

A donates the cross-section, $\rho_{(z)}$ represents the mass density per unit volume of the functionally-graded beam, and U is the strain energy of the functionally-graded beam. \vec{v}^p and \vec{a}^p are velocity and acceleration of the generic point, P , respectively.

The velocity of generic point P can be obtained as

$$\vec{v}^p = \vec{v}^O + \frac{A d\vec{p}}{dt} + \vec{\omega}^A \times \vec{p}; \quad (10)$$

where \vec{v}^O is the velocity of point O , which was a reference point identifying a point fixed in the rigid frame A . $\vec{\omega}^A$ is the angular velocity of the frame A , and \vec{P} is the vector from point O to P . The term $\frac{A d\vec{p}}{dt}$ was the time derivative of the vector \vec{P} in the reference frame A , and the terms \vec{P} , \vec{v}^O , and $\vec{\omega}^A$ can be expressed as follows:

$$\vec{p} = (x + u)\hat{i} + v\hat{j} + w\hat{k}; \quad (11)$$

$$\vec{v}^O = r\Omega\hat{j}; \quad (12)$$

$$\vec{\omega}^A = \Omega\hat{k}; \quad (13)$$

and

$$\vec{v}^p = (\dot{u} - \Omega v)\hat{i} + [\dot{v} + \Omega(r + x + u)]\hat{j} + \dot{w}\hat{k}; \quad (14)$$

where \hat{i} , \hat{j} , and \hat{k} are the orthogonal unit vectors fixed in A , and r is the distance from the axis of rotation to point O (i.e., the radius of the rigid frame). Ω is the angular speed of the rigid frame.

To derive the equations of motion, the partial derivative of the velocity of P , with respect to the generalized speed, q_{ij} s can be obtained as:

$$\frac{\partial \vec{v}^p}{\partial \dot{q}_{1i}} = \phi_{1i}\hat{i}, \quad (i = 1, 2, 3, \dots, \mu_1); \quad (15)$$

where a symbol with a prime ($'$) represents the partial derivative of the symbol with respect to the integral domain variable.

By differentiating Eq. (14) with respect to time, the acceleration of the point P can be obtained as follows in Eq. 18.

Based on the assumptions, the total elastic strain energy of a functionally-graded beam can be written as in Eq. (19), where

$$J_{11}^E = \int_A E_{(z)} dA; \quad (20)$$

$$J_{22,yy}^E = \int_A E_{(z)} z^2 dA; \quad (21)$$

and

$$J_{22,zz}^E = \int_A E_{(z)} y^2 dA. \quad (22)$$

Eq. (20) is axial rigidity, and Eqs. (21) and (22) are the flexural rigidities of the functionally-graded beam.

Substituting the partial velocities and the strain energy expression of Eq. (19) in to Eq. (8), the linearized equations of motion can be obtained as in Eqs. (23) to (25), where a symbol with double prime ($''$) represents the second derivative of the symbol with respect to the integral domain variable.

3. ANALYSIS OF CHORD-WISE NATURAL FREQUENCIES

Eq. (24) governs the chord-wise bending vibration of the functionally-graded rotating beam, which was coupled with Eq. (23). With the assumptions that the first natural frequencies of the stretching motion were far greater than the bending motion, and the coupling effect become negligible for the slender beams,²² the stretching equation of motion and coupling terms involved in Eq. (24) were ignored. The equation can be thus modified as in Eq. (26).

Equation (26) involves the parameters $E_{(z)}$, $\rho_{(z)}$, L , Ω , and x , which are the properties varied along the transverse direction of the beam.

$$s = u + \frac{1}{2} \int_0^x \left[\left(\frac{\partial v}{\partial \sigma} \right)^2 + \left(\frac{\partial w}{\partial \sigma} \right)^2 \right] d\sigma + (\text{Higher Degree Terms}); \tag{6}$$

$$\dot{s} = \dot{u} + \int_0^x \left[\left(\frac{\partial \dot{v}}{\partial \sigma} \right) \left(\frac{\partial v}{\partial \sigma} \right) + \left(\frac{\partial \dot{w}}{\partial \sigma} \right) \left(\frac{\partial w}{\partial \sigma} \right) \right] d\sigma + (\text{Higher Degree Terms}). \tag{7}$$

For the analysis, the equations in the dimensionless form may be obtained by introducing the following dimensionless variables in the equation:

$$\tau \triangleq \frac{t}{T}; \tag{27}$$

$$\xi \triangleq \frac{x}{L}; \tag{28}$$

$$\theta_j \triangleq \frac{q_j}{L}; \tag{29}$$

$$\delta \triangleq \frac{r}{L}; \tag{30}$$

$$\gamma \triangleq T\Omega; \tag{31}$$

where τ , σ , and γ are the dimensionless time, the hub radius ratio, and the dimensionless angular speed, respectively.

After introducing the dimensionless variable from Eq. (27) into Eq. (31) in Eq. (26), the equation can be modified to the Eq. (32), where

$$T = \left(\frac{J_{11}^\rho L^4}{J_{22,ZZ}^E} \right)^{\frac{1}{2}}. \tag{32}$$

Equation (32) can be written as

$$\sum_{j=1}^{\mu_2} \left[M_{ij}^{22} \ddot{\theta}_{2j} + K_{ij}^{B2} \theta_{2j} + \gamma^2 (K_{ij}^{G2} - M_{ij}^{22}) \theta_{2j} \right] = 0, \tag{33}$$

where

$$M_{ij}^{ab} \triangleq \int_0^1 \psi_{ai} \psi_{bj} d\xi; \tag{34}$$

$$K_{ij}^{Ba} \triangleq \int_0^1 \psi''_{ai} \psi''_{aj} d\xi; \tag{35}$$

and

$$K_{ij}^{Ga} \triangleq \int_0^1 (1-\xi) \psi'_{ai} \psi'_{aj} d\xi + \frac{1}{2} \int_0^1 (1-\xi^2) \psi'_{ai} \psi'_{aj} d\xi. \tag{36}$$

In the above equations, ψ_{ai} is a function of ξ and has the same functional value of x .

From Eq. (34), an eigenvalue problem was derived by assuming that θ_s were harmonic functions of τ , expressed as

$$\theta = e^{j\omega\tau} \Theta; \tag{37}$$

where j is the imaginary number, ω is the ratio of the flap-wise bending natural frequency to the reference frequency, and θ is

a constant column matrix characterizing the deflection shape for synchronous motion. The above yields:

$$\omega^2 M \Theta = K^C \Theta; \tag{38}$$

where M is the mass matrix and K^C is the stiffness matrix, which consists of elements defined as:

$$M_{ij} \triangleq M_{ij}^{22}, \tag{39}$$

and

$$K_{ij}^C \triangleq K_{ij}^{B2} + \gamma^2 (K_{ij}^{G2} - M_{ij}^{22}). \tag{40}$$

4. ANALYSIS OF FLAP-WISE NATURAL FREQUENCIES

Equation (25) governed the flap-wise bending vibration of the functionally-graded, rotating beam, which was not coupled with Eqs. (23) and (24). The Equation (25) involved the parameters $E_{(z)}$, $\rho_{(z)}$, L , Ω , and x , in which the properties may vary along the transverse direction of the beam.

The equations in the dimensionless form were obtained by introducing the dimensionless variable from Eq. (27) into Eq. (31) in Eq. (25), resulting in Eq. (42), where

$$T \triangleq \left(\frac{J_{11}^\rho L^4}{J_{22,YY}^E} \right)^{\frac{1}{2}}; \tag{41}$$

From Eq. (43), the eigenvalue problem for the flap-wise bending vibration of the functionally-graded, rotating cantilever beam can be formulated as:

$$\omega^2 M \Theta = K^F \Theta; \tag{42}$$

where M and K^F are defined as

$$M_{ij} \triangleq M_{ij}^{33}; \tag{43}$$

and

$$K_{ij}^F \triangleq K_{ij}^{B3} + \gamma^2 K_{ij}^{G3}. \tag{44}$$

5. NUMERICAL RESULTS AND DISCUSSION

The numerical testing of the procedure, as well as the parametric studies, were performed with two examples in order to establish the validity and application of the present approach to estimate the chord-wise bending vibrations of a functionally-graded, rotating beam, whose properties are given in Table 1.

From Eq. (1), it can be inferred that if $P_m = P_c$, then there was no variation in the properties across the section, implying the beam was made up of fully metallic material.

$$\frac{\partial \vec{v}^P}{\partial \dot{q}_{2i}} = \left[-\sum_0^{\mu_2} \left(\int_0^x \phi'_{2i} \phi'_{2j} d\sigma \right) q_{2j} \right] \hat{i} + \phi_{2i} \hat{j}, \quad (i = 1, 2, 3, \dots, \mu_2); \quad (16)$$

$$\frac{\partial \vec{v}^P}{\partial \dot{q}_{3i}} = \left[-\sum_0^{\mu_3} \left(\int_0^x \phi'_{3i} \phi'_{3j} d\sigma \right) q_{3j} \right] \hat{i} + \phi_{3i} \hat{k}, \quad (i = 1, 2, 3, \dots, \mu_3); \quad (17)$$

$$\vec{a}^P = [\ddot{u} - 2\Omega\dot{v} - \Omega^2(r + x + u)]\hat{i} + [\ddot{v} + 2\Omega\dot{u}(r + x + u)]\hat{j} + \ddot{w}\hat{k}; \quad (18)$$

$$U = \frac{1}{2} J_{11}^E \int_L \left(\frac{ds}{dx} \right)^2 dx + \frac{1}{2} J_{22,zz}^E \int_L \left(\frac{d^2 v}{dx^2} \right)^2 dx + \frac{1}{2} J_{22,yy}^E \int_L \left(\frac{d^2 w}{dx^2} \right)^2 dx; \quad (19)$$

$$\begin{aligned} & \sum_{j=1}^{\mu_1} \left[\left(\int_0^L J_{11}^p \phi_{1i} \phi_{1j} dx \right) \ddot{q}_{1j} - 2\Omega \left(\int_0^L J_{11}^p \phi_{1i} \phi_{2j} dx \right) \dot{q}_{2j} - \Omega^2 \left(\int_0^L J_{11}^p \phi_{1i} \phi_{1j} dx \right) q_{1j} + \left(\int_0^L J_{11}^E \phi'_{1i} \phi'_{1j} dx \right) q_{1j} \right] \\ & = \Omega^2 \int_0^L J_{11}^p x \phi_{1i} dx + r\Omega^2 \int_0^L J_{11}^p \phi_{1i} dx; \end{aligned} \quad (23)$$

$$\begin{aligned} & \sum_{j=1}^{\mu_2} \left[\left(\int_0^L J_{11}^p \phi_{2i} \phi_{2j} dx \right) \ddot{q}_{2j} - \Omega^2 \left(\int_0^L J_{11}^p \phi_{2i} \phi_{2j} dx \right) q_{2j} + \left(J_{22,zz}^E \int_0^L \phi''_{2i} \phi''_{2j} dx \right) q_{2j} \right. \\ & \quad \left. + \Omega^2 \left\{ r \left(\int_0^L J_{11}^p (L-x) \phi'_{2i} \phi'_{2j} dx \right) q_{2j} + \left(\int_0^L \frac{J_{11}^p}{2} (L^2 - x^2) \phi'_{2i} \phi'_{2j} dx \right) q_{2j} \right\} \right. \\ & \quad \left. + 2\Omega \left(\int_0^L J_{11}^p \phi_{2i} \phi_{1j} dx \right) \dot{q}_{1j} \right] = 0; \end{aligned} \quad (24)$$

$$\begin{aligned} & \sum_{j=1}^{\mu_3} \left[\left(\int_0^L J_{11}^p \phi_{3i} \phi_{3j} dx \right) \ddot{q}_{3j} + \left(J_{22,yy}^E \int_0^L \phi''_{3i} \phi''_{3j} dx \right) q_{3j} \right. \\ & \quad \left. + \Omega^2 \left\{ r \left(\int_0^L J_{11}^p (L-x) \phi'_{3i} \phi'_{3j} dx \right) q_{3j} + \left(\int_0^L \frac{J_{11}^p}{2} (L^2 - x^2) \phi'_{3i} \phi'_{3j} dx \right) q_{3j} \right\} \right] = 0; \end{aligned} \quad (25)$$

$$\begin{aligned} & \sum_{j=1}^{\mu_2} \left[\left(\int_0^L J_{11}^p \phi_{2i} \phi_{2j} dx \right) \ddot{q}_{2j} - \Omega^2 \left(\int_0^L J_{11}^p \phi_{2i} \phi_{2j} dx \right) q_{2j} + \left(J_{22,zz}^E \int_0^L \phi''_{2i} \phi''_{2j} dx \right) q_{2j} \right. \\ & \quad \left. + \Omega^2 \left\{ r \left(\int_0^L J_{11}^p (L-x) \phi'_{2i} \phi'_{2j} dx \right) q_{2j} + \left(\int_0^L \frac{J_{11}^p}{2} (L^2 - x^2) \phi'_{2i} \phi'_{2j} dx \right) q_{2j} \right\} \right] = 0; \end{aligned} \quad (26)$$

$$\begin{aligned} & \sum_{j=1}^{\mu_2} \left[\frac{J_{11}^p L^4}{T^2} \left(\int_0^1 \psi_{2i} \psi_{2j} d\zeta \right) \ddot{\theta}_{2j} + J_{22,zz}^E \left(\int_0^1 \psi''_{2i} \psi''_{2j} d\zeta \right) \theta_{2j} \right. \\ & \quad \left. + \frac{J_{11}^p L^4}{T^2} \gamma^2 \left\{ \delta \left(\int_0^1 (1-\zeta) \psi'_{2i} \psi'_{2j} d\zeta \right) \theta_{2j} + \frac{1}{2} \left(\int_0^1 (1-\zeta^2) \psi'_{2i} \psi'_{2j} d\zeta \right) \theta_{2j} - \left(\int_0^1 \psi_{2i} \psi_{2j} d\zeta \right) \theta_{2j} \right\} \right] = 0. \end{aligned} \quad (32)$$

$$\sum_{j=1}^{\mu_3} \left[\frac{J_{11}^{\rho} L^4}{T^2} \left(\int_0^1 \psi_{ai} \psi_{bj} d\zeta \right) \ddot{\theta}_{3j} + J_{22,yy}^E \left(\int_0^1 \psi''_{ai} \psi''_{bj} d\zeta \right) \theta_{3j} \right. \\ \left. + \frac{J_{11}^{\rho} L^4}{T^2} \gamma^2 \left\{ \delta \left(\int_0^1 (1-\zeta) \psi'_{ai} \psi'_{bj} d\zeta \right) \theta_{3j} + \frac{1}{2} \left(\int_0^1 (1-\zeta^2) \psi'_{ai} \psi'_{bj} d\zeta \right) \theta_{3j} \right\} \right] = 0; \quad (42)$$

$$\sum_{j=1}^{\mu_3} \left[M_{ij}^{33} \ddot{\theta}_{3j} + K_{ij}^{B3} \theta_{3j} + \gamma^2 K_{ij}^{G3} \theta_{3j} \right] = 0. \quad (43)$$

Table 1: Properties of metallic (Steel) and ceramic (Alumina) materials.

Properties of materials	Steel	Alumina(Al_2O_3)
Youngs modulus E [Gpa]	214.00	390.00
Material density ρ [$\frac{kg}{m^3}$]	7800.00	3200.00

Table 2: Comparison of natural frequencies of a metallic (Steel) cantilever beam (H_z).

Present Approach	Analytical ²⁸	Experimental ²⁸
96.9	96.9	97.0
607.3	607.6	610.0
1700.4	1699.0	1693.0

Example 1

In Table 2, the first three chord-wise bending natural frequencies of the functionally-graded beam were obtained using the present modelling method. They were then compared with those from earlier works, based on the finite element method²⁸ and experimental data.²⁹ The assumptions in the study were that the beam was metallic with a power law index, $n \rightarrow \text{inf}$ (i.e., steel), and had the following geometrical dimensions: breadth = 22.12mm, height = 2.66mm, and length = 152.40mm. The material properties are provided in Table 1.

At zero rotational speed, with clamped free (clamped at $x = 0$ and free at $x = L$) boundary conditions, the chord-wise bending natural frequencies were calculated with ten assumed modes to obtain the three lowest natural frequencies. The mass matrix and stiffness matrix are presented in the appendix. A comparison of the results obtained with those reported in the literature^{28,29} indicated that deviation was less than 0.5%.

Example 2

A functionally-graded non-rotating beam with dimensions length $L = 1000mm$, breadth = 20mm, and height = 10mm was considered for this analysis. Steel was considered as the metallic constituent, and alumina was used as the ceramic constituent (the mechanical properties are given in Table 1).

In Fig. (2), the variation of the lowest three chord-wise bending natural frequencies of a functionally-graded beam with respect to the power law index, n , was presented and compared to the results.²⁸ It was observed that chord-wise bending natural frequencies decreased while n value increased. When the beam composition approached a more metallic state, the frequencies became asymptotic to the power law index axis. The

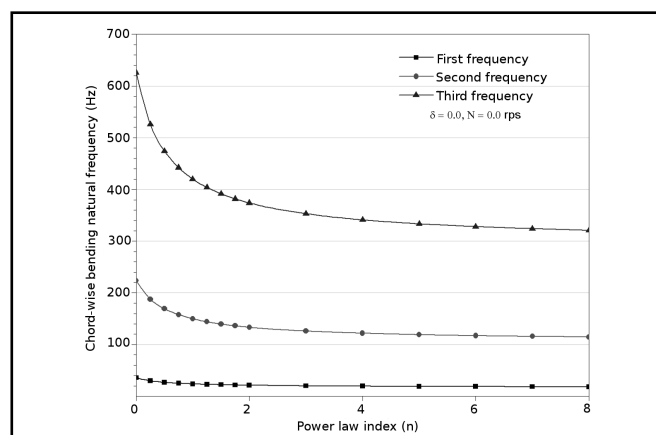


Figure 2: Variation of chord-wise bending natural frequencies of non rotating functionally-graded beam.

present observations were in conformity with the results reported, wherein the shear effect was considered.²⁸ Although the present approach did not take into account the shear component, the present observations were in conformity with those made in earlier studies, where, it had been reported that the influence of the shear was negligible at the lower order frequencies.^{14,30}

From the above examples, it may be concluded that the present modelling method is appropriate for further evaluation. In this light, further analysis has been carried out for a beam with the same dimensions and functionally-graded properties as in Example 2.

In Figure (3), the variation of the chord-wise bending natural frequencies were plotted against the angular speed of rotation of the beam for the power law index, $n = 0$ (the beam was made of ceramic metal). It has been observed that, the frequencies increased along with an increase in angular speed, for all hub radii ratio. However, the increase in frequencies, as well as rate of increase, has been found to be higher in respect to higher hub radii ratio. The observed behaviour can be attributed to an increase in the centrifugal inertia force, due to increases in hub radius and angular speed.

The relationship between the chord-wise bending natural frequency and the power law index for the different hub radii ratio, at constant angular speed, is presented in Fig. (4). In general, it was observed that the chord-wise bending natural frequencies increased along with an increase in the hub radius ratio; i.e., for a given power law index, a higher hub radius ra-

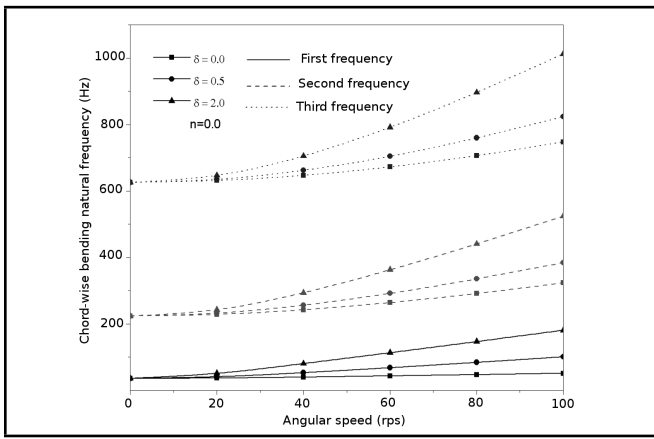


Figure 3: Variation of chord-wise bending natural frequencies with angular speed.

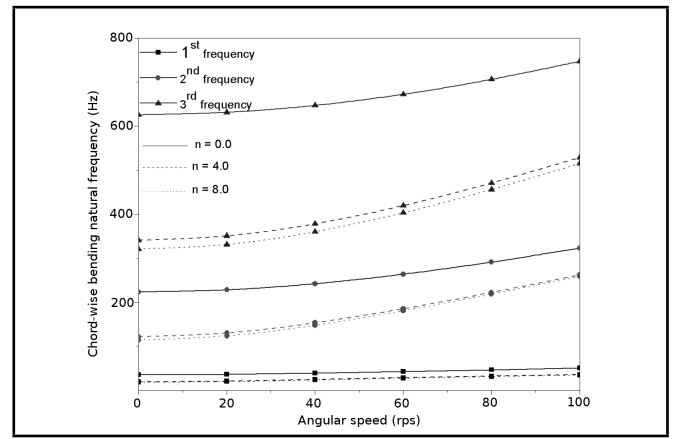


Figure 5: Variation of chord-wise bending natural frequencies with angular speed.

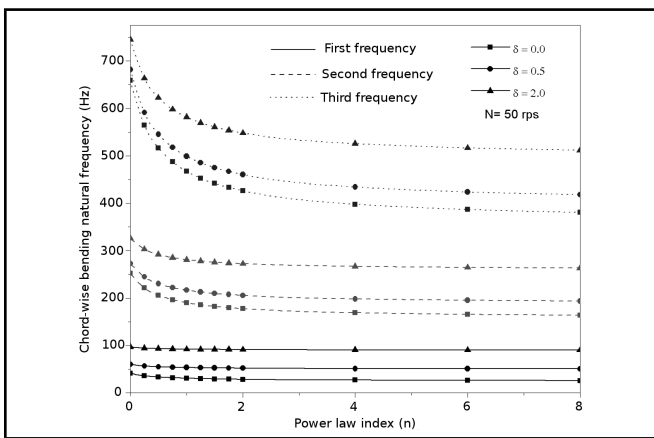


Figure 4: Variation of chord-wise bending natural frequencies with power law index.

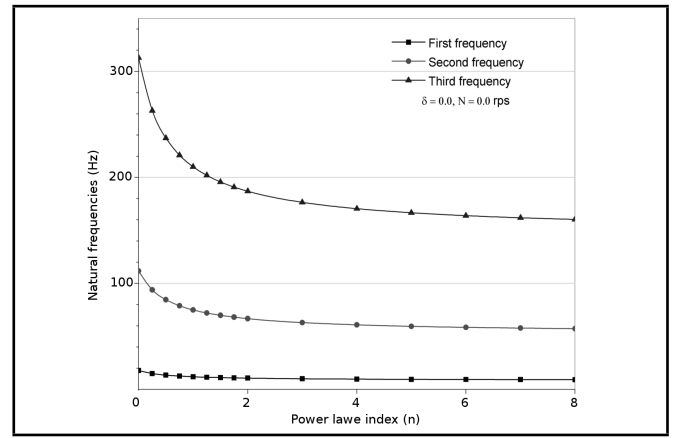


Figure 6: Variation of flap-wise bending natural frequencies of non rotating functionally-graded uniform beam.

tio (delta value) resulted in higher frequency. This behaviour becomes predominant in the following order: third frequency, which was greater than the second frequency, and greater than first frequency. The chord-wise bending natural frequencies of the functionally-graded, rotating beam decreased rapidly as the power law index changed from zero to two. When the beam composition approached fully metallic, the frequencies become asymptotic to the power law index axis.

As the rotating speed of the functionally-graded beam increased, the chord-wise bending natural frequencies increased and the rate of increase in the natural frequency was predominant for the beams with higher power law index, as seen in Fig. (5).

In Table 3, the chord-wise bending natural frequencies were compared to the flap-wise bending natural frequencies. The flap-wise bending natural frequencies obtained from Eq. (43) aligned well with those obtained from the relationship originally introduced.¹

The variation of the lowest three flap-wise bending natural frequencies of a functionally-graded beam, with respect to the power law index, n , are presented in Fig. (6). It was observed that the flap-wise bending natural frequencies of the functionally-graded rotating beam decreased rapidly up to a value of the power law index, and then the frequencies become

asymptotic to the power law index axis. As the rotating speed of the functionally-graded beam increased, the flap-wise bending natural frequencies increased and the rate of increase in natural frequency was predominant for the beams with a higher power law index, as presented in Fig. (7).

For the speed variation between 0 to 100 rps, the rate of increase of chord-wise and flap-wise bending natural frequencies has been evaluated for different values of the power law index, and presented in Figs. (8) and (9) respectively. It has been ob-

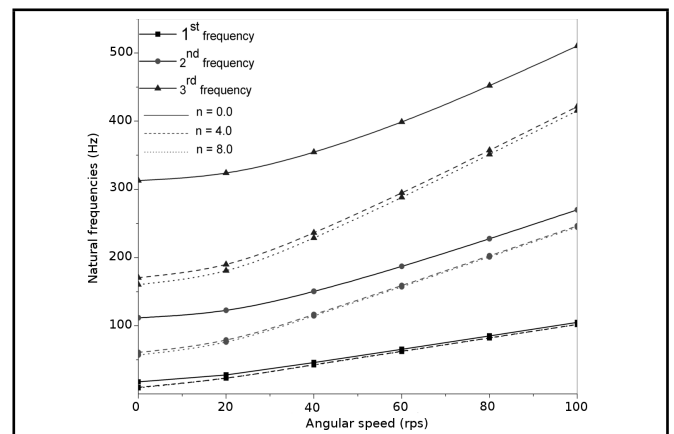


Figure 7: Variation of flap-wise bending natural frequencies with angular speed.

Table 3: Comparison of the first chord-wise natural frequencies (Hz) and the first flap-wise natural frequencies (Hz) at $n = 0, 4$ and 8, for the beam $b = 20mm$ $d = 20mm$ and $L = 1000mm$.

$N(rps)$	$\rho \downarrow$	Chord-wise			Flap-wise from Eq. (36)		
	$n \rightarrow$	0	4	8	0	4	8
2	0.0	35.67792	19.46406	18.30947	35.73393	19.56654	18.41838
	0.5	35.72192	19.54458	18.39505	35.77786	19.64665	18.50345
	2.0	35.85359	19.78417	18.64939	35.90933	19.885	18.75633
25	0.0	37.26551	22.05061	21.00614	44.87447	33.33511	32.65361
	0.5	43.3133	31.10963	30.36529	50.01042	39.91001	39.33257
	2.0	57.72327	49.00565	48.5085	62.9045	55.01413	54.57174
50	0.0	41.1941	26.48727	25.87316	64.7839	56.77268	56.2976
	0.5	60.15645	51.10753	50.55035	78.22275	71.49811	71.1009
	2.0	96.63529	90.70758	90.34597	108.8043	103.5754	103.2589

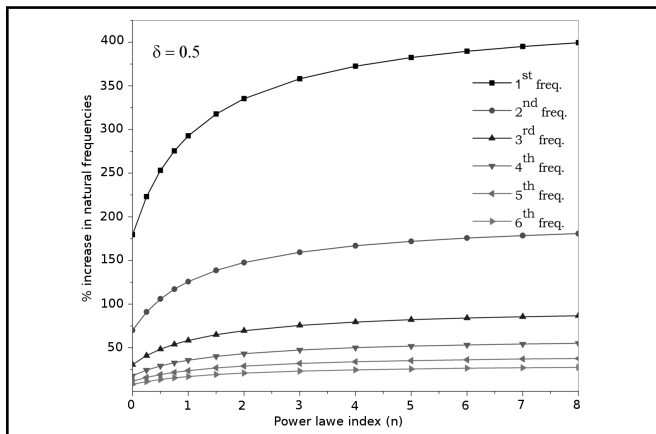


Figure 8: Percentage variation in chord-wise bending natural frequencies with power law index.

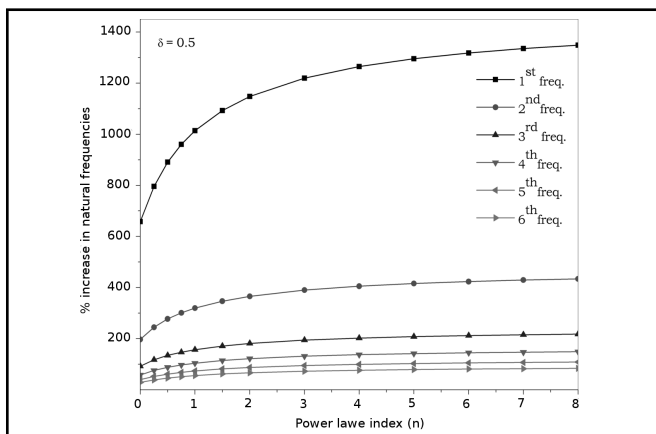


Figure 9: Percentage variation in flap-wise bending natural frequencies with power law index.

served that the increase in frequencies was greater at the lower power law indices. In addition, the effect was predominant in the lower order frequencies. It has also been noted that the percentage increase in the chord-wise bending natural frequency was smaller, when compared to that in flap-wise frequency. At higher values of the power law index, the rate of variation of frequencies with respect to power law index, n , were observed to remain nearly constant.

6. CONCLUSIONS

In this work, the equations of motion were derived for a rotating, functionally-graded, cantilever beam attached to a rigid hub. With the coupling effect ignored, the effects of the power law index, angular speed, and hub radius on the natural frequencies of a functionally-graded, rotating beam were investigated for the bending configuration in chord-wise and flap-wise modes. This was first completed through a numerical study, and then a comparison with the numerical results reported in the literature was conducted. The results showed that the chord-wise and flap-wise bending natural frequencies increased along with the increase in angular speed, due to an increase in the centrifugal inertia force, which increased along with the increase in the angular speed and hub radius ratio. Both the chord-wise and flap-wise bending natural frequencies of the functionally-graded, rotating beam decreased rapidly when the beam morphology changed from ceramic to a ceramic-metal structure. It was also noticed that the increase in the angular speed had a cumulative effect on both the natural frequencies, and was more dominant on the lower frequency modes with a low value of power law index. It was decided that the present modelling approach can usefully be employed for the design and analysis of rotating, functionally-graded beam structures.

REFERENCES

- 1 Naguleswaran, S. Lateral Vibration Of A Centrifugally Tensioned Uniform Euler-Bernoulli Beam, *Journal of Sound and Vibration*, **176**(5), 613–624, (1994).
- 2 Sankar, B.V. An elasticity solution for functionally-graded beams, *Composites Science and Technology*, **61**(5), 689–696, (2001).
- 3 Sina, S.A., Navazi, H.M., and Haddadpour, H. An analytical method for free vibration analysis of functionally-graded beams, *Materials and Designs*, **30**, 741–747, (2009).
- 4 Yang, J., and Chen, Y. Free vibration and buckling analyses of functionally-graded beams with edge cracks, *Composite Structures*, **83**(1), 48–60, (2008).

- 5 Ying, J., Lü, C.F., and Chen, W.Q. Two-dimensional elasticity solutions for functionally-graded beams resting on elastic foundations, *Composite Structures*, **84**(3), 209–219, (2008).
- 6 Li, X.F. A unified approach for analysing static and dynamic behaviors of functionally-graded Timoshenko and Euler-Bernoulli beams, *Journal of Sound and Vibration*, **318**(4-5), 1210–1229, (2008).
- 7 Yang, J., Chen, Y., Xiang, Y., and Jia, X.L. Free and forced vibration of cracked inhomogeneous beams under an axial force and a moving load, *Journal of Sound and Vibration*, **312**(1-2), 166–181, (2008).
- 8 Li, Y., and Shi, Z. Free vibration of a functionally-graded piezoelectric beam via state-space based differential quadrature, *Composite Structures*, **87**(3), 257–264, (2009).
- 9 Kadoli, R., Akhtar, K., and Ganesan, N. Static analysis of functionally-graded beams using higher order shear deformation theory, *Applied Mathematical Modelling*, **32**(12), 2509–2525, (2008).
- 10 Aydogdu, M., and Taskin, V. Free vibration analysis of functionally-graded beams with simply supported edges, *Material Design*, **28**(5), 1651–1656, (2007).
- 11 Kocatürk, T., and Şimşek, M. Vibration of viscoelastic beams subjected to an eccentric compressive force and a concentrated moving harmonic force, *Journal of Sound and Vibration*, **291**(1-2), 302–322, (2006).
- 12 Şimşek, M., and Kocatürk, T. Free and forced vibration of a functionally-graded beam subjected to a concentrated moving harmonic load, *Composite Structures*, **90**(4), 465–473, (2009).
- 13 Kapuria, S., Bhattacharyya, M., and Kumar, A.N. Bending and free vibration response of layered functionally-graded beams: a theoretical model and its experimental validation, *Composite Structures*, **82**(3), 390–402, (2008).
- 14 Jaworski, J.W., and Dowell, E.H. Free vibration of a cantilevered beam with multiple steps: Comparison of several theoretical methods with experiment, *Journal of Sound and Vibration*, **312**(4-5), 713–725, (2008).
- 15 Kang, Y.-A., and Li, X.-F. Bending of functionally-graded cantilever beam with power-law non-linearity subjected to an end force, *International Journal of Non-Linear Mechanics*, **44**(6), 696–703, (2009).
- 16 Benatta, M.A., Mechab, I., Tounsi, A., and Adda Bedia, E.A. Static analysis of functionally-graded short beams including warping and shear deformation effects, *Computational Materials Science*, **44**(2), 765–773, (2008).
- 17 Şimşek, M. Static analysis of a functionally-graded beam under a uniformly distributed load by Ritz method, *International Journal of Engineering and Applied Science*, **92**(4), 904–917, (2009).
- 18 Şimşek, M. Vibration analysis of a functionally-graded beam under a moving mass by using different beam theories, *Composite Structures*, **92**(4), 904–917, (2010).
- 19 Ozdemir Ozgumus, O., and Kaya, M.O. Vibration analysis of a rotating tapered Timoshenko beam using DTM, *Mechanica*, **45**(1), 33–42, (2010).
- 20 Chih-Ling Huang, W.-Y.L., and Kuo-Mo H. Free flapping vibration of rotating inclined Euler beams, *World Academy of Science, Engineering and Technology*, **32**, 7, (2009).
- 21 Huang, C.L., Lin, W.Y., and Hsiao, K.M. Free vibration analysis of rotating Euler beams at high angular velocity, *Computers and Structures*, **88**(17-18), 991–1001, (2010).
- 22 Yoo, H.H., and Shin, S.H. Vibration analysis of rotating cantilever beams, *Journal of Sound and Vibration*, **212**(5), 807–828, (1998).
- 23 Yoo, H.H., Ryan, R.R., and Scott, R.A. Dynamics of flexible beams undergoing overall motions, *Journal of Sound and Vibration*, **181**(2), 261–278, (1995).
- 24 Park, J.-H., Park, H.-Y., Jeong, S.-Y., Lee, S.-I., Shin, Y.-H., and Park, J.-P. Linear vibration analysis of rotating wind-turbine blade, *Current Applied Physics*, **10**(2, supplement), S332–S334, (2010).
- 25 Alshorbagy, A.E., Eltaher, M.A., and Mahmoud, F.F. Free vibration characteristics of a functionally-graded beam by finite element method, *Applied Mathematical Modelling*, **35**(1), 412–425, (2011).
- 26 Fazlzadeh, S.A., Malekzadeh, P., Zahedinejad, P., and Hosseini, M. Vibration analysis of functionally-graded thin-walled rotating blades under high temperature supersonic flow using the differential quadrature method, *Journal of Sound and Vibration*, **306**(1-2), 333–348, (2007).
- 27 Fazlzadeh, S.A., and Hosseini, M. Aerothermoelastic behavior of supersonic rotating thin-walled beams made of functionally-graded materials, *Journal of Fluids and Structures*, **23**(8), 1251–1264, (2007).
- 28 Piovan, M.T., and Sampaio, R. A study on the dynamics of rotating beams with functionally-graded properties, *Journal of Sound and Vibration*, **327**(1-2), 134–143, (2009).
- 29 Carnegie, W., and Dawson, B. Vibration characteristics of straight blades of asymmetrical aerofoil cross-section, *The Aeronautical Quarterly*, 178, (1963).
- 30 Rao, S.S., and Gupta, R.S. Finite element vibration analysis of rotating Timoshenko beams, *Journal of Sound and Vibration*, **242**(1), 103–124, (2001).

$$K_{ij} = \int_0^1 \psi''_{ai} \psi''_{bj} d\zeta + \gamma^2 \left(\delta \int_0^1 (1 - \zeta) \psi'_{ai} \psi'_{bj} d\zeta + \frac{1}{2} \int_0^1 (1 - \xi^2) \psi'_{ai} \psi'_{aj} d\xi \right); \tag{A2}$$

where $i, j = 1, 2, 3 \dots 10$.

$$M = \begin{bmatrix} 1.0000e+00 & 2.6724e-09 & 8.9146e-10 & 1.7774e-09 & -2.9703e-10 & -2.2329e-12 & -8.3807e-12 & -2.8567e-11 & -4.4917e-11 & 1.8673e-09 \\ 2.6724e-09 & 1.0000e+00 & -1.3992e-09 & -1.7475e-09 & 2.6855e-10 & 1.6532e-11 & 1.0925e-12 & 2.8145e-11 & 3.6804e-11 & -1.6434e-09 \\ 8.9146e-10 & -1.3992e-09 & 1.0000e+00 & 2.7141e-09 & -4.2182e-10 & 3.7260e-11 & -2.8419e-11 & -9.0184e-12 & -4.1115e-11 & 1.4541e-09 \\ 1.7774e-09 & -1.7475e-09 & 2.7141e-09 & 1.0000e+00 & 5.5667e-10 & -3.5111e-10 & 1.5390e-10 & -1.0486e-10 & 2.2785e-11 & 1.2263e-09 \\ -2.9703e-10 & 2.6855e-10 & -4.2182e-10 & -5.5667e-10 & 1.0000e+00 & -2.4532e-10 & 7.7767e-11 & -5.7360e-11 & -4.0586e-13 & 1.0693e-09 \\ -2.2329e-12 & 1.6532e-11 & 3.7260e-11 & 3.5111e-10 & -2.4532e-10 & 1.0000e+00 & 1.9502e-11 & 9.1972e-12 & 2.2916e-11 & -9.2911e-10 \\ -8.3807e-12 & 1.0925e-12 & -2.8419e-11 & -1.5390e-10 & 7.7767e-11 & 1.9502e-11 & 1.0000e+00 & -1.7600e-11 & -1.5859e-11 & 7.8972e-10 \\ -2.8567e-11 & 2.8145e-11 & -9.0184e-12 & 1.0486e-10 & -5.7360e-11 & 9.1972e-12 & -1.7600e-11 & 1.0000e+00 & 1.2049e-11 & -6.6831e-10 \\ -4.4917e-11 & 3.6804e-11 & -4.1115e-11 & -2.2785e-11 & -4.0586e-13 & 2.2916e-11 & -1.5859e-11 & 1.2049e-11 & 1.0000e+00 & 5.7914e-10 \\ 1.8673e-09 & -1.6434e-09 & 1.4541e-09 & -1.2263e-09 & 1.0693e-09 & -9.2911e-10 & 7.8972e-10 & -6.6831e-10 & 5.7914e-10 & 1.0000e+00 \end{bmatrix}; \tag{A3}$$

$$K = \begin{bmatrix} 1.2362e+1 & 6.7005e-8 & -2.2947e-8 & 5.5941e-8 & -3.7640e-8 & 3.3940e-8 & -3.4069e-8 & 3.3543e-8 & -3.4256e-8 & 6.8658e-8 \\ 6.7005e-8 & 4.8552e+2 & -1.9098e-6 & 3.8206e-7 & -1.1001e-6 & 1.2385e-6 & -1.2300e-6 & 1.2466e-6 & -1.2217e-6 & 3.1009e-8 \\ -2.2947e-8 & -1.9098e-6 & 3.8065e+3 & 1.3748e-5 & -5.0220e-6 & 3.5581e-6 & -3.5240e-6 & 3.3661e-6 & -3.5113e-6 & 1.1726e-5 \\ 5.5941e-8 & 3.8206e-7 & 1.3748e-5 & 1.4617e+4 & -3.4062e-5 & 3.1058e-5 & -2.8177e-5 & 2.7509e-5 & -2.6460e-5 & -1.2573e-6 \\ -3.7640e-8 & -1.1001e-6 & -5.0220e-6 & -3.4062e-5 & 3.9944e+4 & -2.1626e-5 & 1.4937e-5 & -1.4231e-5 & 1.2274e-5 & 5.2677e-5 \\ 3.3940e-8 & 1.2385e-6 & 3.5581e-6 & 3.1058e-5 & -2.1626e-5 & 8.9135e+4 & 1.9759e-6 & 7.8093e-7 & 1.4227e-6 & -1.2468e-4 \\ -3.4069e-8 & -1.2300e-6 & -3.5240e-6 & -2.8177e-5 & 1.4937e-5 & 1.9759e-6 & 1.7388e+5 & -4.8040e-6 & 7.1768e-8 & 2.0511e-4 \\ 3.3543e-8 & 1.2466e-6 & 3.3661e-6 & 2.7509e-5 & -1.4231e-5 & 7.8093e-7 & -4.8040e-6 & 3.0821e+5 & -6.5849e-7 & -3.0665e-4 \\ -3.4256e-8 & -1.2217e-6 & -3.5113e-6 & -2.6460e-5 & 1.2274e-5 & 1.4227e-6 & 7.1768e-8 & -6.5849e-7 & 5.0848e+5 & 4.3866e-4 \\ 6.8658e-8 & 3.1009e-8 & 1.1726e-5 & -1.2573e-6 & 5.2677e-5 & -1.2468e-4 & 2.0511e-4 & -3.0665e-4 & 4.3866e-4 & 7.9340e+5 \end{bmatrix}; \tag{A4}$$

$$K = \begin{bmatrix} 3.3646e+2 & -1.4873e+2 & -2.8537e+2 & -2.2280e+2 & -1.9229e+2 & -1.6305e+2 & -1.4327e+2 & -1.2651e+2 & -1.1381e+2 & -1.0299e+2 \\ -1.4873e+2 & 2.6985e+3 & 3.8380e+2 & -2.8297e+2 & -7.7886e+2 & -8.1031e+2 & -7.0940e+2 & -6.7090e+2 & -6.0629e+2 & -5.6722e+2 \\ -2.8537e+2 & 3.8380e+2 & 1.0294e+4 & 1.9388e+3 & -1.9860e+3 & -1.3953e+3 & -1.7091e+3 & -1.4798e+3 & -1.4951e+3 & -1.3559e+3 \\ -2.2280e+2 & -2.8297e+2 & 1.9388e+3 & 2.8025e+4 & 4.5293e+3 & -3.0033e+3 & -1.8492e+3 & -2.6447e+3 & -2.2350e+3 & -2.3990e+3 \\ -1.9229e+2 & -7.7886e+2 & -1.9860e+3 & 4.5293e+3 & 6.2818e+4 & 8.1089e+3 & -4.0607e+3 & -2.1556e+3 & -3.5924e+3 & -2.9399e+3 \\ -1.6305e+2 & -8.1031e+2 & -1.3953e+3 & -3.0033e+3 & 8.1089e+3 & 1.2403e+5 & 1.2670e+4 & -5.1560e+3 & -2.3226e+3 & -4.5405e+3 \\ -1.4327e+2 & -7.0940e+2 & -1.7091e+3 & -1.8492e+3 & -4.0607e+3 & 1.2670e+4 & 2.2336e+5 & 1.8210e+4 & -6.2919e+3 & -2.3589e+3 \\ -1.2651e+2 & -6.7090e+2 & -1.4798e+3 & -2.6447e+3 & -2.1556e+3 & -5.1560e+3 & 1.8210e+4 & 3.7483e+5 & 2.4724e+4 & -7.4703e+3 \\ -1.1381e+2 & -6.0629e+2 & -1.4951e+3 & -2.2350e+3 & -3.5924e+3 & -2.3226e+3 & -6.2919e+3 & 2.4724e+4 & 5.9480e+5 & 3.2213e+4 \\ -1.0299e+2 & -5.6722e+2 & -1.3559e+3 & -2.3990e+3 & -2.9399e+3 & -4.5405e+3 & -2.3589e+3 & -7.4703e+3 & 3.2213e+4 & 9.0198e+5 \end{bmatrix}. \tag{A5}$$

APPENDIX

For the vibration analysis, several assumed modes that which satisfy the boundary conditions of the cantilever beam can be used to construct the mass and stiffness matrices in Eqs. (36) and (45).

For the functionally-graded beam considered in the first example, the elements of mass matrix and the stiffness matrix for ten modes can be estimated from: the relations

$$M_{ij} = \int_0^1 \psi_{2i} \psi_{2j} d\zeta; \tag{A1}$$

where $i, j = 1, 2, 3 \dots 10$; and from Eq. (A2) (see above).

Using the Eqs. (A1) and Eq. (A2), the mass matrix and the stiffness matrix for a non-rotating, cantilever beam can be obtained as Eqs. (A3), and (A4).

The stiffness matrix for the rotating functionally-graded beam at $N = 100rps$, $n = 0$, and $\delta = 2.0$ was Eq. (A5)